RESEARCH

The Effect of Counterbody Material on Tribological Behavior of Active Screen Plasma-Nitrided Inconel 718 Under Saline Solution

Yukyhiro I. Oikava[1] · Bruna C. E. S. Kurelo[1] · Giuseppe Pintaude[1] · Viviane T. Mazur[2] · Xiaoying Li[3] · Hanshan Dong[3]

Abstract

Considering the relevance of Inconel 718 alloy for the oil and gas industry and the nature of the tribological system to define the friction and wear behaviors during sliding, this investigation presents results obtained in reciprocating tests under saline solution for active-screen plasma-nitrided Inconel 718. Bearing steel and silicon nitride ceramic were used as counterbodies, balls of 4 mm diameter. Extensive plastic deformation was confirmed using nanoindentation analysis, and oxidation governed the tribological responses when the steel ball was used as a counterbody. In these conditions, the presence of a nitrided layer was significant in reducing wear by one order of magnitude. On the other hand, when the ceramic ball was tested, abrasive wear was the primary mechanism, and the nitrided layer did not affect either the friction or the wear rate of Inconel 718. The corrosion behavior helped to confirm the predominance of described wear mechanisms.

Graphical abstract
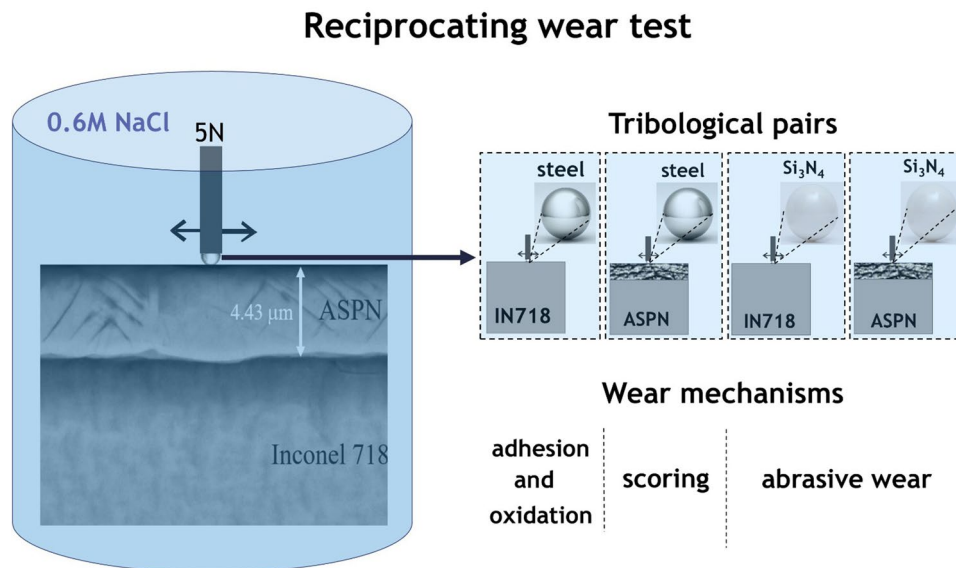
✉ Giuseppe Pintaude
pintaude@utfpr.edu.br

1   Universidade Tecnológica Federal do Paraná, Campus Curitiba, Curitiba 81280-340, Brazil

2   Universidade Tecnológica Federal do Paraná, Campus Guarapuava, Guarapuava 85015-430, Brazil

3   The University of Birmingham, Birmingham B15 2TT, UK

1 Introduction

Nickel alloys manufacture many components in the oil and gas industry. In particular, the Inconel 718 alloy has mainly been used due to its resistance to hydrogen embrittlement

[1]. However, many components, such as stem valves, are subject to heavy contact pressures involving friction. The worst consequence is the seizure of parts [2], considering the possibility of similar materials coming into contact.

Many attempts have been proposed to mitigate the wear damages on Inconel 718. Among them, nitriding of this alloy has been conducted in different ways: gas nitriding [3], liquid nitriding [4], and plasma nitriding [5–8]. The last process can be performed under different systems, including glow discharge [5], hot wall DC-pulsed power [6], arc-enhanced glow discharge [7], and intensified plasma [8]. To our knowledge, anyone had used active screen plasma nitriding (ASPN) to modify the surface of Inconel 718.

Ni-based alloys are recognized as difficult-to-cut materials. To surpass the challenges involved with subtractive manufacturing [9], Inconel 718 has been processed using Additive Manufacturing techniques (AM), such as laser powder bed fusion [10]. Although Stachowiak et al. [10] described a better tribocorrosion behavior of Inconel 718 processed using AM than the conventional route, the mechanical component still needed to be significantly improved using the alternative processing. Besides, post-treatments can be a proper solution to modify the microstructure of Inconel 718 processed by AM, implying additional costs to improve its corrosion resistance [11]. Therefore, choosing AM for Inconel alloys is not an obvious selection to achieve a good balance between wear and corrosion.

On the other hand, applying a thermochemical treatment is a promising alternative to increase the wear resistance of conventional corrosion resistance alloys, such as duplex stainless steels [12]. For localized corrosion, low-temperature plasma nitriding conducted in a pulsed cold wall DC reactor improved the resistance of Inconel 718, as verified by de la Rosa et al. [13]. However, Refs. [10] and [13] did not evaluate the effect of different natures of tribological pairs during the wear processes.

In this fashion, Houghton et al. [2] verified a positive answer of plasma nitriding during ball-on-ring tests under dry conditions, using plasma nitriding to increase the load capacity of Inconel 718 to postpone seizure initiation. Although their investigation considered similar and different tribological pairs, the plasma nitrided layer must be thoroughly characterized, making it difficult to interpret its role. Since the tribological pair can be composed of materials with different mechanical properties, wear mechanisms depend on the difference between bodies [14, 15].

In the context of reducing the wear of Inconel 718 using active screen plasma nitriding, this investigation aims to verify the effect of different counterbodies on the tribological behavior of this alloy under a saline solution interfacial medium.

2 Experimental Procedure

2.1 Material and Nitriding Processing

Inconel 718 was used as a substrate, and its chemical composition (in wt%) of Inconel 718 was 53.5% Ni, 18.6% Cr, 5.0% Nb, 2.88% Mo, 1.02% Ti, 0.52% Al, 0.015% C and the balance in Fe. Solubilization was conducted for 1 h at 1090 °C, and an aging process at 788 °C for 7 h was employed for the raw material.

Samples with 34 mm × 27 mm × 7 mm were finished up to 1200-mesh sandpaper (Sq = 0.081 ± 0.007 μm). Then, the active screen plasma nitriding (ASPN) was carried out at 400 °C for 20 h, using a gas mixture of 75% nitrogen and 25% hydrogen in an AS Plasma Metal 75 kVA industrial scale unit. The selection of low temperatures is to avoid the formation of CrN precipitates, which can compromise the corrosion performance [16]. After nitriding processes, the treated surfaces' Sq parameter (Root Mean Square Height) was 0.153 ± 0.004 μm. X-ray analyses were performed using CuKα radiation, a current of 30 mA, a voltage of 40 kV, a glazing angle of 5°, and scanned at 0.02°/s from 2θ of 30° to 100°.

The Vickers hardness values of studied specimens were measured by applying for 10 s a load of 5 g. Besides, the hardness and elastic modulus of the tested surfaces were measured by nanoindentation with the Quasi Continuous Stiffness Measurement (QCSM) method. A maximum load of 100 mN was applied using a Berkovich tip rounding was ~ 200 nm. Calibration details are described elsewhere [17]. Twenty indentations were performed with a spacing of 30 μm between them on the surfaces and on the counterbodies balls before and after the wear test. After the tests, the contact stiffness technique was applied [18] to minimize the effects of roughness on the loading curves.

2.2 Reciprocating Wear Testing

The reciprocating tests were performed in a tribometer with a load cell of 10 N capacity. Two different balls were used as counterbody: (i) AISI 52100 steel and (ii) Si_3N_4 ceramic ball, both with 4 mm diameter, moving under 5 Hz of

Table 1 Designation of tribological pairs tested under saline solution

Ball material (counterbody)	Tested specimen	Designation of pair
52,100 steel	Inconel 718	IN718-S
52,100 steel	Nitrided Inconel 718	ASPN-S
Si_3N_4	Inconel 718	IN718-c
Si_3N_4	Nitrided Inconel 718	ASPN-c

frequency. The normal load was 5 N, the track distance was 5 mm, and the testing time was 1800s. This time was sufficient to reach the steady state in both samples. Additional tests were also carried out with 300 or 900 s to investigate the evolution of wear mechanisms. During the reciprocating tests, the specimens were submerged in artificial saline solution (0.6 M NaCl) interfacial media, using a proper container, described elsewhere under ring-on-cylinder lubricated tests [19], without recirculation. Each test setup was repeated three times, at least.

The coefficient of friction (COF) was determined by measuring the tangential force with a frequency of 1 Hz. Only the steady-state regime was considered to calculate the average values, discharging the initial high fluctuations due to static friction. This regime was confirmed after we checked the same pattern of friction curves observed either after 300 s or after 1800s.

The worn tracks were studied using an optical interferometer, using a sampling resolution of 1024×1024 points. The wear volume was determined using the tools' stitching' and 'volume of a hole/peak' through Taly Map Platinum 6.1 software. Any filter besides leveling was applied to the measured surfaces.

The four tribological pairs will be identified following the nomenclature presented in Table 1.

2.3 Corrosion Characterization

The corrosion tests were performed in an aerated solution of 0.6 M NaCl at 25 ± 1 °C. Flat plate samples were used as working electrodes, assembling in the bottom of the nylon electrochemical cell, where a hole of 1 cm diameter exposes an area of 0.785 cm^2, sealed with O-rings, and fixed with clamps. All specimens were sanded using 600-mesh SiC to characterize the corrosion parameters (OCP, E_{cor}, Rp, I_{cor}, and corrosion rate) without the surface roughness effect. After sanding, they were washed in water and dried before
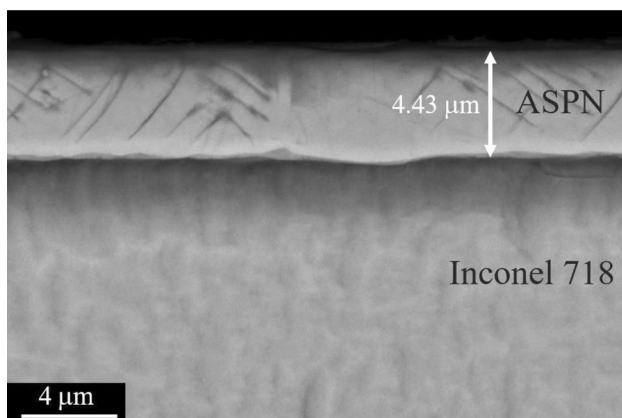

Fig. 1 Transversal section of nitrided layer obtained in Inconel 718
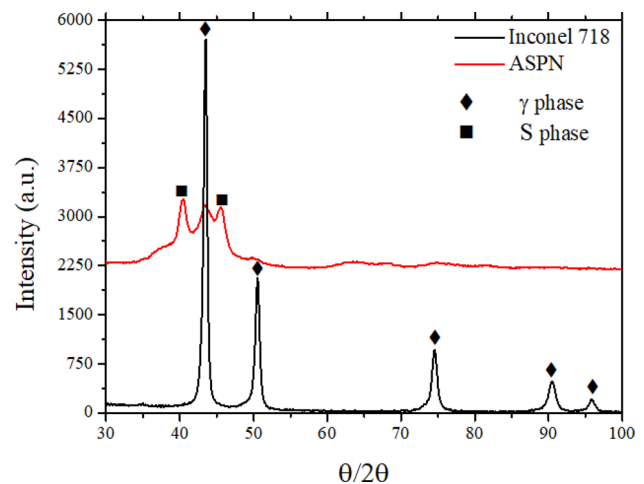

Fig. 2 XRD spectra of Inconel 718 and nitrided layer

assembling on the electrochemical cell. Open circuit potentials (OCP) were measured and determined after 3300 s of immersion, as recommended by the ASTM G-59–97 standard [20], using a potentiostat system connected to a microcomputer. The micro and macropolarization tests were carried out by disturbing the system in ± 10 mV around E_{cor} and ± 150 mV, respectively, using a scan speed of 1 mV s^{-1}. The E_{cor} was determined accordingly to the macropolarization curves. A platinum counter-electrode and an Ag/AgCl reference electrode were used. Three runs were performed to obtain the average values.

3 Results and Discussion

3.1 Characterization of Tested Materials

A nitrided layer 4.43 μm thick was formed on the surface of the Inconel 718 in the sample ASPN (Fig. 1).

The nitrided layer contains slip lines, resulting from a significant lattice expansion. The same feature was described by Jing et al. [16] after the salt bath nitriding of Inconel 718. The surface roughness of the untreated specimen increased. Many investigations [5–8] reported increased surface roughness after nitriding, including values closer to those described here [6]. Maniee et al. [6] claimed an explanation based on the formation and coarsening of precipitates using hot wall plasma nitriding. The precipitation cannot be applied to our case (Fig. 2), but the findings of Ref. [13] showed that a higher nitriding temperature did not increase the Sq parameter. On the other hand, they revealed a grain boundaries pattern after nitriding at 400 ℃, most probable to increase the peaks predominance. For these reasons, the swelling is the most probable reason for increasing roughness, following the technique applied by Stinville et al. [21]

Table 2 Tribological responses after reciprocating tests with 52,100 steel as counterbody

Pair	COF	Wear rate [mm^3/N m] $\times 10^{-5}$	H^3/E'^{2} [GPa]
IN718-S	0.29 ± 0.01	0.98 ± 0.2	0.005
ASPN-S	0.36 ± 0.03	0.09 ± 0.02	0.036

The onset of plastic deformation is indicated by H^3/E'^{2}

after nitriding, confirmed further in the case of Ni-base alloys [22].

Figure 2 shows that only the gamma phase was detected in the X-ray spectrum and determined to be Inconel 718. With the plasma nitriding, S-phase was developed, corresponding to the peaks at 40.4° and 45.6°. The reduction in the intensity of the $\gamma_{(200)}$ peak was also observed by Jing et al. [16], who used salt bath nitriding at 425 °C for different times (4, 8, and 16 h). As expected, any nitride precipitate was formed after active screen plasma nitriding.

Regarding the microhardness, the nitrided specimens had an average value of 1200 ± 100 HV$_{0.005}$, while the substrate material (IN718) in its aged condition reached 530 ± 10 HV$_{0.005}$. The Berkovich measurements also showed an increase in surface hardness after plasma nitriding with a mean value of 12.1 ± 0.5 GPa and the untreated surface with a mean value of 5.9 ± 0.1 GPa. The elastic moduli determined were 204 ± 7 GPa and 222 ± 5 GPa, for Inconel and plasma nitrided surface, respectively. These elastic modulus values are in the same order of magnitude as those reported by Kovací et al. [5].

3.2 Tests with AISI 52100 Steel Balls

Table 2 shows the average values of COF and wear rates determined to Inconel 718 and ASPN samples after reciprocating tests against AISI 52100 steel balls.

The ASPN treatment effectively reduced the wear rate of Inconel 718 alloy under the investigated conditions. On the other hand, the COF value obtained for the IN718-S pair is

Fig. 3 Worn tracks of IN718 (**a**, **b**, and **c**) and ASPN samples (**d**, **e**, and **f**) after reciprocating tests against steel ball. Note intense plastic deformation and discontinuous oxide layer in the IN718 sample and scratches in the ASPN sample
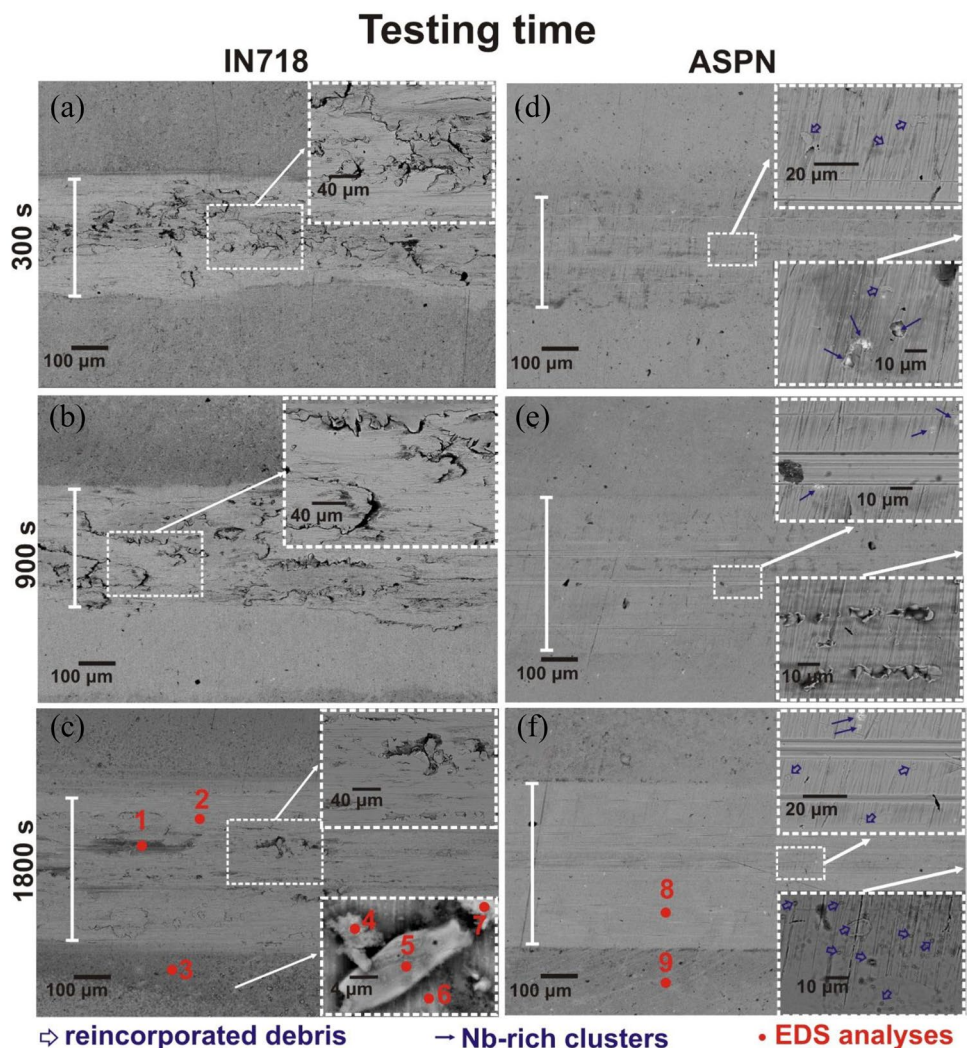
the lowest in the current investigation. The reasons for friction and wear are different because the interface developed during the wear process differs.

The hardness of the steel ball is higher than Inconel 718 but lower than the ASPN sample. Considering the reduced modulus E' to estimate the load to initiate the plastic deformation on the flat surface [23], Table 2 shows that the value of H^3/E'^2 of the ASPN sample is one order of magnitude higher than that calculated for Inconel alloy. Then, the plastic deformation caused by the steel ball on the Inconel surface should be higher, which was reflected in the resulting wear rate.

The plastic deformation was observed on worn tracks of Inconel 718, associated with a considerable amount of adhered material, resulting from the successive contacts during the reciprocating movement (Fig. 3).

The worn surface of IN718 (Fig. 3a) shows that at the beginning of sliding (300 s of testing time), wear debris

has a significant adhesion onto the wear track. Looking at the widths of worn surfaces, it is notable the increase from 900 to 1800s of testing time (Fig. 3b and c). Along with the adhesion mechanism, an oxidation process happened due to the presence of chloride ions. The EDS analysis performed on point 1 confirms the presence of oxygen. On the other hand, under brighter regions, represented by point 2, the oxides probably were removed. The local chemical analysis on point 3, which is rich in oxygen, is proof of the ejection of oxides. The oxidation had occurred in debris also: the EDS analysis showed a more significant oxygen content in points 4, 5, and 7 than in point 6 (worn surface).

Identifying wear debris after tests conducted with ASPN samples was much more difficult. In Fig. 3d and e, it is possible to see that the width of the wear track increased up to 900 s of testing time, meaning a reduced time to reach the steady-state regime of wear compared to tests with IN718. The reason for that is the change of predominant wear
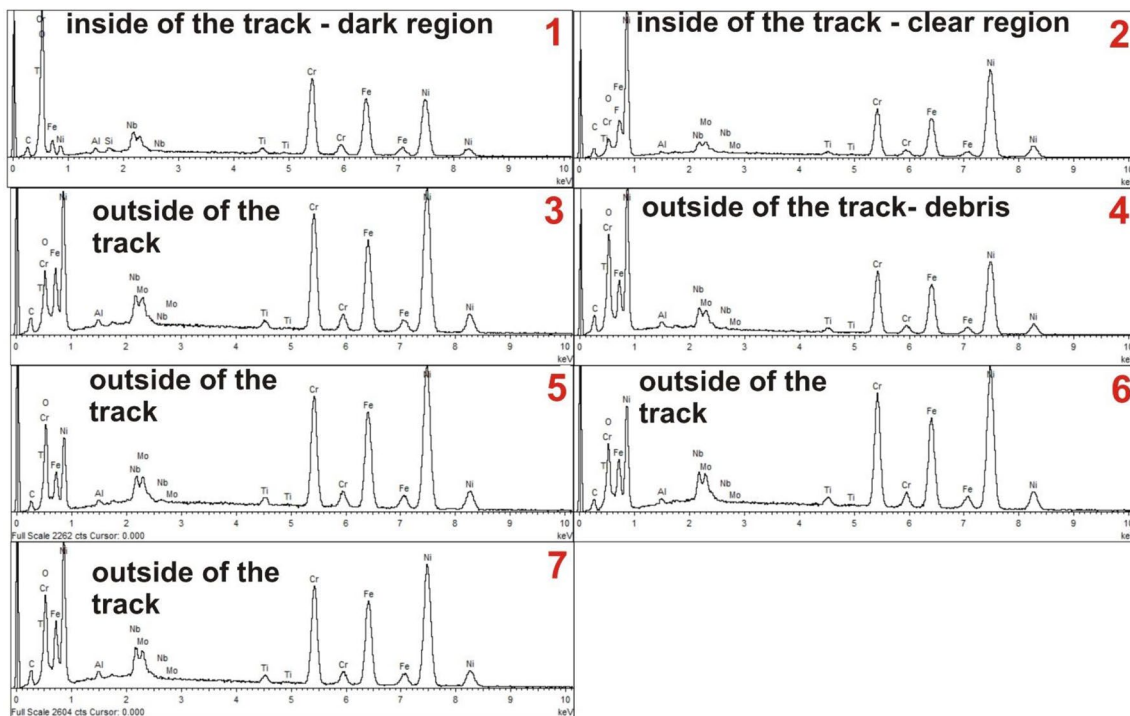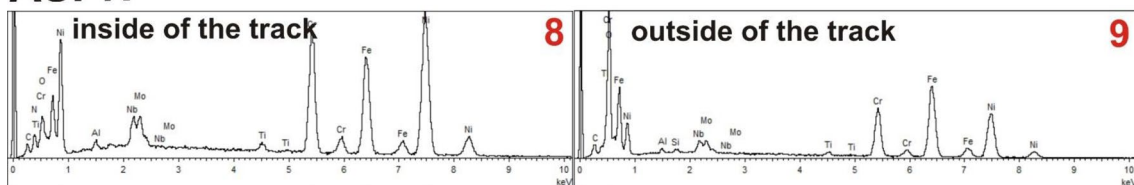

Fig. 4 EDX spectra for points inside and outside worn tracks of IN718 (1 to 7) and ASPN samples (8 and 9) after reciprocating tests against steel ball
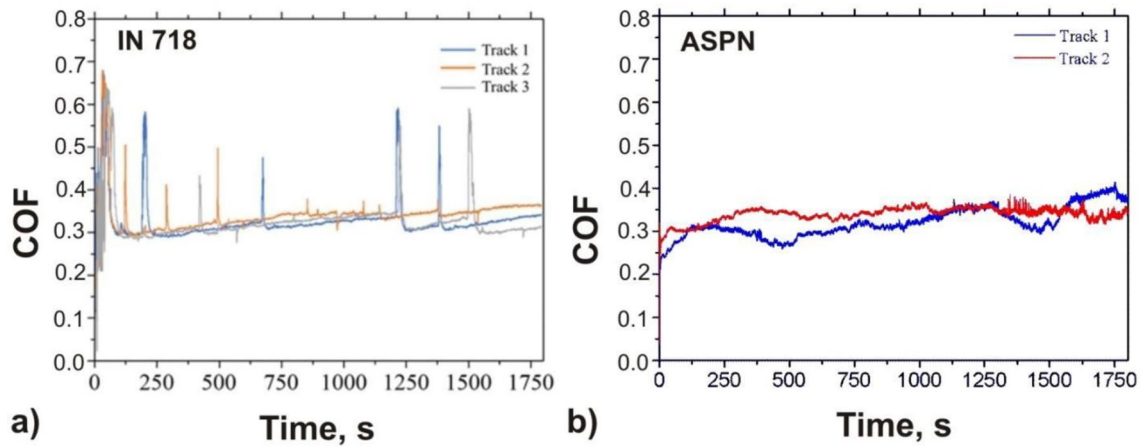
Fig. 5 Friction evolution along with testing time: **a** IN718-S pair, and **b** ASPN-S pair
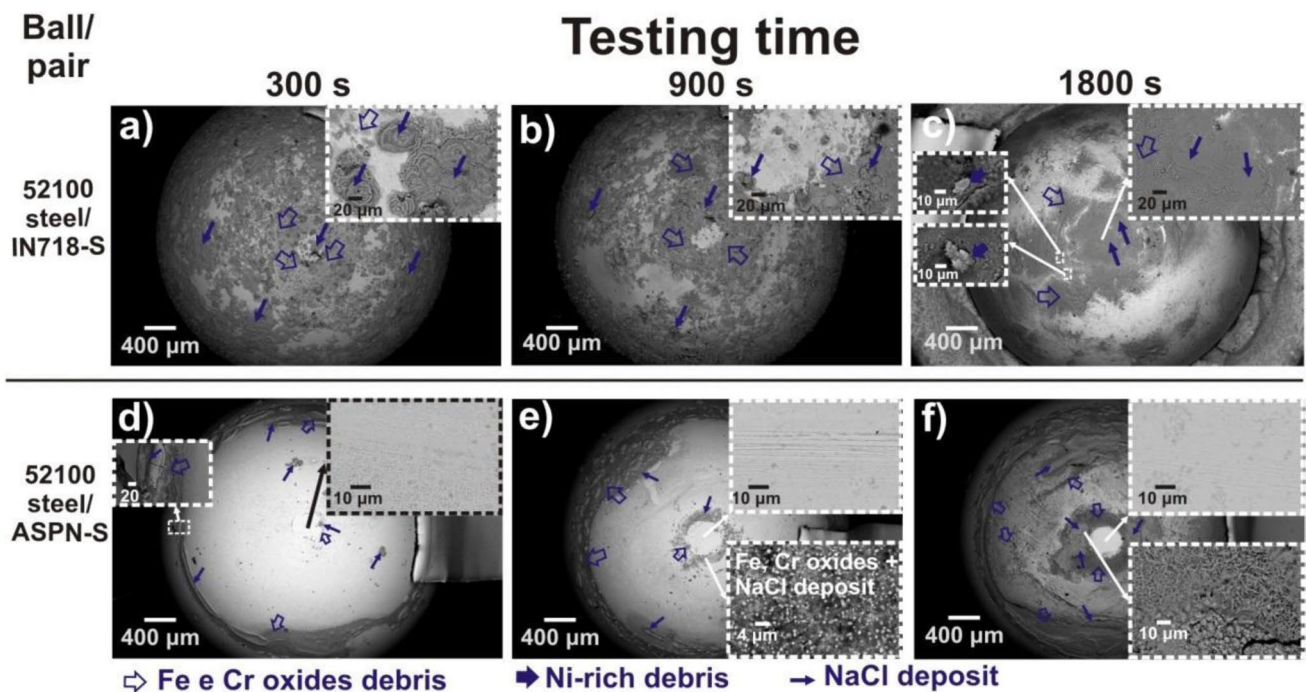

Fig. 6 SEM images of steel ball after reciprocating tests with IN718 and ASPN samples: **a** and **d** after 300 s, **b** and **e** after 900 s, **c** and **f** after 1800 s of testing time. Note intense oxidation, Ni-rich debris, and NaCl deposit

mechanism: adhesion was much less intense in the presence of a nitride layer; conversely, besides the Nb-rich clusters identified using EDS, the worn surfaces present scratches. During the sliding process, these particles were pulled out; they can roll and attach to the counterbody, as illustrated in the insets presented in Fig. 3d and e. This process can happen in the IN718 sample but be much more intense in ASPN, where the wear was much lesser. The EDS analysis helped to identify a more extensive content of oxygen and iron outside the track (point 9) than inside (point 8), indicating a higher presence of oxides expelled from the sliding track.

The corresponding EDX spectra determined for points indicated in Fig. 3, inside and outside worn tracks, are presented in Fig. 4 (points 1 to 9).

The average friction curve for the IN718-S pair (Fig. 5a) shows intense and immediate peaks throughout with whole testing time. They represent the collapse of tribofilm formed on the 52,100 steel balls, illustrated in Fig. 6a, b, and c. Additionally to the discontinuous tribofilm, it is worthwhile that the surfaces of the balls did not flat during the wear process; therefore, they kept acting as an indenter agent to the Inconel 718. Thus, the contact stresses developed during
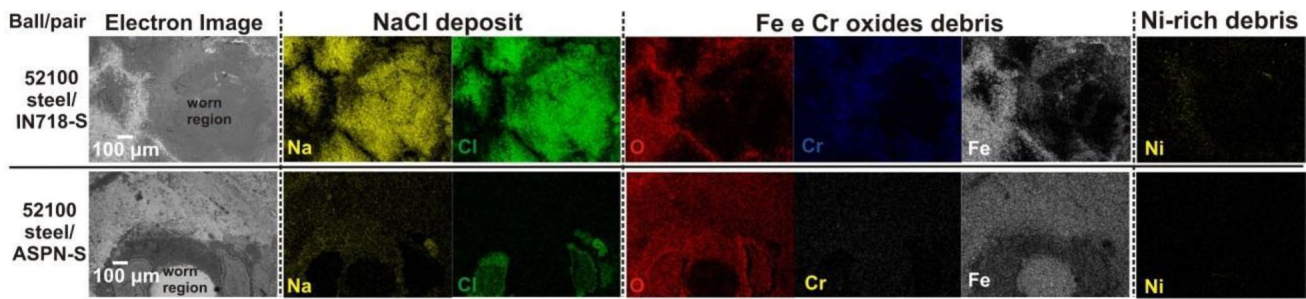
Fig. 7 EDS maps of the worn 52,100 steel balls after 1800s of testing time. NaCl deposits, oxides, and Ni-rich debris are detected

Table 3 Hardness (GPa) of different tribo-elements and strain hardening (%) after tests with IN718-S and ASPN-S tribo-pairs

Tribo-pair	Sample	Unworn surface, GPa	Worn surface after 900 s of testing time, GPa	Variation in hardness, %
IN718-S	IN718 (body)	5.9 ± 0.1	7 ± 1	18.6
IN718-S	52,100 steel (counterbody)	12.3 ± 0.3	13 ± 2.5	5.7
ASPN-S	ASPN (body)	12.1 ± 0.5	13.9 ± 0.5	15.3
ASPN-S	52,100 steel (counterbody)	12.3 ± 0.3	14.8 ± 0.8	20.3

the wear process can only remove the tribofilm, and further adhesion and ejection processes are expected for third bodies, maintaining the steady-state regime, as postulated by Fillot et al. [24]. This tribofilm combines iron oxide, NaCl, and adhered materials from Inconel. The presence of saline solution caused the oxidation of the steel surface, but the maintenance of oxide depends on the level of contact pressure. During the period when the oxide predominated, the level of COF values was below ~ 0.3. Conversely, friction levels determined by Maniee et al. [5] for dry contact between Inconel 718 and 52,100 steel is close to 1, where probably any oxide layer could be kept whole at the interface.

As verified in other investigations [7, 25], iron oxides can reduce friction. Mondragón-Rodríguez et al. [7] found COF of ~ 0.25 for Inconel 718 and 52,100 steel balls under pin-on-disk experiments. Although their contact pressure is relatively close to that used here, their conditions of velocity and configuration promoted oxidation. However, these authors revealed only the oxide layer on the disk surfaces.

The friction became stable and higher when contact was established between the steel ball and the ASPN surface (Fig. 5b). The presence of the tribofilm was insufficient to reduce the COF values, which occurred due to the higher wear of the steel ball, as illustrated in Fig. 6d, e, and f. One can note the flattening of balls, which is a phenomenon that changes the contact pressure and is expected when the indenter body is softer than its counterface [26]. Besides, the difference between the polarization resistances of steel

Table 4 Tribological responses after reciprocating tests with silicon nitride as counterbody

Pair	COF	Wear rate $[mm^3/N\ m] \times 10^{-5}$
IN718-c	0.37 ± 0.03	2.5 ± 0.6
ASPN-c	0.39 ± 0.01	2.1 ± 0.5

and a nitrided surface should be considered. Basu et al. [27] determined that the plasma nitriding can double it. Therefore, the tendency to form oxide layers might be restricted to the steel surface.

Looking at the worn surface of the steel ball after contact with the ASPN surface, the region of contact is metallic, and a discontinuous tribofilm, with fewer amounts of Na and Cl—can be observed (Fig. 6). The intense deformation broke the layer, and most probably small debris can enter the interface. The maximum value of hardness for an iron oxide as a product of corrosion determined by Chicot et al. [28] is 5.3 GPa. There needs to be more than this value to scratch the ASPN surface. Considering this fact, the most probable abrasive agent is a mixed layer, including the severely work-hardened surface of the steel ball.

Figure 7 illustrates the worn surfaces of balls after tests; they contain NaCl deposits, oxides layers, and
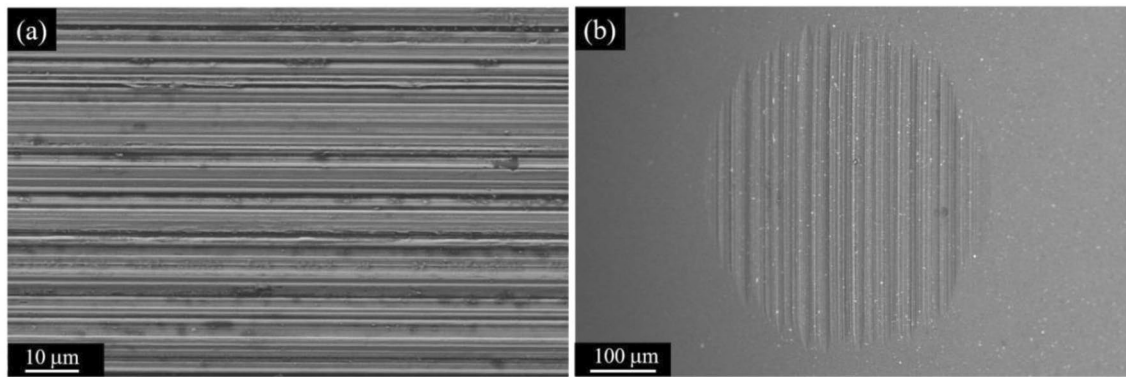
Fig. 8 a Worn track of Inconel 718 sample after reciprocating tests against silicon nitride. Note oriented grooves; and **b** SEM image silicon nitride ball after reciprocating tests in the same condition
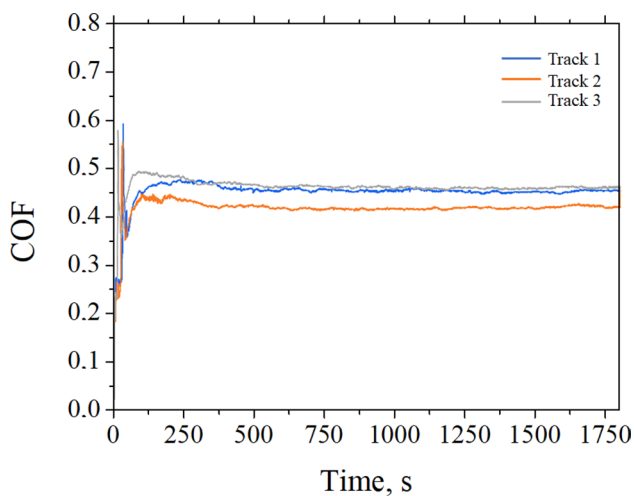

Fig. 9 Friction evolution along with the testing time of IN718-c pair

3.3 Tests with Silicon Nitride Balls

Table 4 shows the average values of COF and wear rates determined for Inconel 718 and ASPN samples after reciprocating tests against silicon nitride balls.

The presence of a nitrided layer, when Inconel was worn by silicon nitride, was insignificant for friction coefficient and wear rate. Regarding the standard deviations, the performance with or without plasma nitriding can be similar.

The reason for that is the observed wear mechanism on the worn surfaces, similar to when IN718 and ASPN samples were tested against silicon nitride. As shown in Fig. 8a, directional scratches can be observed after reciprocating tests. The same pattern of scratches was identified on the silicon nitride surface, which can be observed in Fig. 8b.

The friction curves (Fig. 9) show a relevant transient period in which the COF is higher than that determined for steady-state one. In the case of Inconel 718 samples, this transient period was accompanied by a high fluctuation in the COF values, meaning a significant change in the interface nature. This aspect is essential to identify the abrasive agent, besides the harder asperities of silicon nitride.

We can find in the literature that a significant work-hardening occurs when Ni-alloys are in contact with harder counterbodies. Papageorgiou et al. [30] conducted tribocorrosion experiments to verify the responses of NiCrMo-625 alloy. This material was subject to 6 to 70 N (916 to 2078 MPa of average contact pressures) in a ball-on-flat reciprocating system, using a polycrystalline alumina ball of 6 mm diameter as a counterpart. They verified an increase in hardness on worn tracks of approximately 37% under the lowest applied load. Besides, the alumina ball presented more considerable wear.

Based on this description, we can infer that the plastic deformation of the worn track is achieved in the initial

Ni-rich debris at the surfaces. Pintaude et al. [29] determined the hardness after abrasion of 52,100 steel as 14.1 GPa. In this case, and considering the probable small size of debris, these work-hardened particles would be able to scratch the ASPN surfaces.

Measuring the work hardening through nanoindentation (Table 3), we can observe a higher value than determined by Ref. [29] for the worn surface of the steel ball against the ASPN surface (14.8 GPa). The intensity of cold working was small (12.8 GPa) when testing IN718 because the plastic deformation of this body was predominant (18.6% increase), as discussed previously and confirmed by looking at the results of Table 3.

In this situation, the minor wear of the ASPN surface can also be checked by the maintenance in average roughness after wear testing. Its value of the Sq parameter was reduced by only 4%, meaning the surface scoring was the primary mechanism in this testing condition.

Table 5 Electrochemical parameters obtained in the corrosion tests under 0.6 M NaCl solution

Material	OCP [mV]	E_{cor} [mV]	Rp [Ohm]$\times 10^5$	I_{cor} [nA/cm^2]	Corrosion rate [mm/year]$\times 10^{-4}$
Inconel 718	-117 ± 35	-136 ± 25	4 ± 1	33.6 ± 32.7	3.4 ± 3.3
ASPN	-55 ± 7	-72 ± 6	4 ± 1	14.7 ± 0.07	1.49 ± 0.08
52,100 steel[a]	Non-informed	-765	0.089	13,900	5502

[a]Data from Ref. [27]
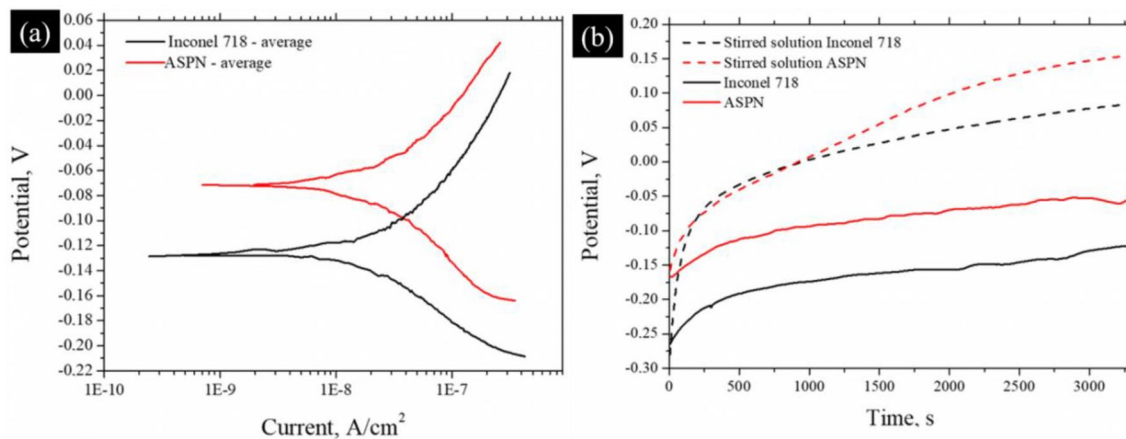
Fig. 10 **a** Polarization curves obtained to Inconel 718 and ASPN samples; **b** Evolution of open circuit potential (0.6 M NaCl solution)

periods, accompanied by a high transfer of materials from part to part. After that, the formed tribofilm can scar both balls and the tested sample.

The insignificant effect of a nitrided layer under these conditions was also verified elsewhere. Espallargas and Mischler [31] investigated the tribological responses of pulsed plasma nitrided Ni–Cr alloy using 15 N of applied load in a ball on a flat system. Under a solution of 0.5 M H_2SO_4, they concluded that the same mechanical wear rates were found for untreated and treated materials.

Considering the microabrasion as the resulting mechanism in tests performed with silicon nitride, comparing our results with others obtained under the microscale abrasion test seems reasonable. Varela et al. [32] compared the performance of Inconel 625 with and without plasma nitriding. Their results showed that the performance of untreated Inconel did not differ much from that reported for nitrided surface because the standard deviation determined to nitrided condition was relatively large. Due to its higher hardness, the wear resistance of Inconel 718 can be higher than that determined for Inconel 625. Therefore, for our case, the more negligible difference can be justified for this reason, and of course, for the differences in thickness and microstructure of the nitrided layer.

4 Discussion on Corrosion and Tribocorrosion Effects

Table 5 presents the electrochemical parameters for Inconel 718 and ASPN specimens using 0.6 M NaCl solution (Fig. 10a shows the average polarization curves).

The determined results in polarization regarding E_{cor}, I_{cor}, and corrosion rate agree with those described in Ref. [6] for untreated Inconel 718 and nitrided surfaces. Unfortunately, Refs. [6] and [27] did not present the standard deviations of corrosion parameters, which would be helpful. As expected, the corrosion behavior resulting from the nitriding process could be improved about Inconel 718.

A question arises from observing all worn tracks, considering the presence of artificial saline solution at the interface. In what tested system this solution made a real difference? To our understanding, only when the counterpart suffered intense corrosion and a formed tribofilm could act to change the friction, i.e., the IN718-S pair. In other studied cases, the mechanical wear was much more intense than corrosive wear.

The change in friction during tribocorrosion was studied by Jun et al. [33]. Using alumina as a pin, they investigated the tribological behavior of NiCrMo-625 nickel-based alloy in a pin-on-disk. These researchers concluded that the COF
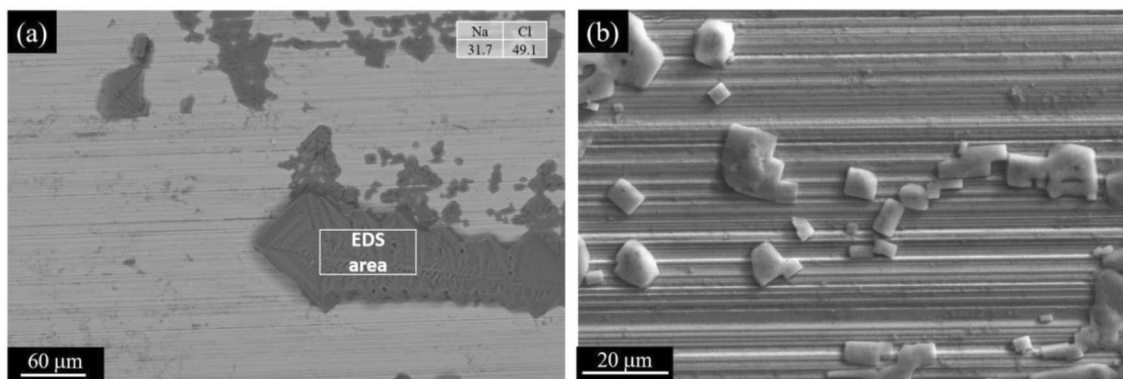
Fig. 11 **a** NaCl tribofilm formed at ASPN surface after tests with Si$_3$N$_4$; and **b** NaCl debris observed in the same tribological pair (ASPN-c)

of NiCrMo-625 alloy shows a slightly decreasing trend with increasing potential in the range of − 1.0 to 1.0 V. Friction signal presented high fluctuations due to the formation and cracking of oxide layers. This behavior implies high wear in tests conducted with positive potential.

However, their remarkable result was determining the material loss caused by corrosion without wear. Under − 0.5 V, this result was nil; even under OCP, the proportion with pure mechanical wear was only 0.02%.

To verify what the OCP would be closer to the situation experimented on during the wear tests, we verified the effect of agitation on OCP. The solution was stirred with a helix-shaped paddle made of polymeric material (LDPE) using a cc electric motor at 33 rpm.

In Fig. 10b, one can see that the potentials shifted quickly from negative to positive values under stirred solutions. The effect of agitation on OCP and its relation with tribocorrosion was analyzed by López-Ortega et al. [34]. They concluded that the effect of agitation is considerable on non-passivating steel and negligible on a passive one.

Our results show that both Inconel and nitrided layers have the same behavior; therefore, all differences in tribocorrosion can be input to the steel counterbody, which is a non-passive material. In this sense, using hard and corrosion-resistant ceramics as counterbodies can disturb the performance analysis of metallic and treated surfaces. Kasturibai and Kalaignan [35] showed that introducing Si$_3$N$_4$ nanoparticles in Ni can reduce the up to 70 times the corrosion rate. Besides the harder asperities of Si$_3$N$_4$, its presence isolated the NaCl from the aqueous solution. We observed this effect on the worn surfaces of the ASPN-c pair, shown in Fig. 11.

Finally, we mention the investigation conducted by Woodward et al. [36], who tested pins of cast iron against disks of AISI 4330 and 15-5PH steels under saline solution. They observed that NaCl solution acted as a lubricant, compared with dry tests, instead of increasing the total wear. The differences between the wear of dissimilar materials of disks

can be considered insignificant, which reinforces the discussion about the effect of counterbody on the tribocorrosion behavior. For future investigations, we recommend using non-passive bodies, considering their passivation behavior to model the wear components, mechanical and corrosive.

5 Conclusions

Active screen plasma-nitriding was conducted at low-temperature at the surface of Inconel 718, forming a single layer of S-phase. Its tribological behavior was studied in a reciprocating system under saline solution, varying the counterbody material. Based on the described results, the following conclusion can be put forward:

– When a deformable and non-passive counterbody—52,100 steel—is used, the nitrided layer significantly reduced the wear, but the friction behavior was governed by the tribofilm formation and its partial maintenance, which is verified during the contact between steel and untreated Inconel 718;
– The use of a ceramic counterbody—silicon nitride ball—results in an abrasion mechanism of wear; in this case, the presence of a nitrided layer was insignificant for both wear and friction results; and
– Tribocorrosion approaches should consider non-passive counterbodies to express the representative contacts and practical mechanical and corrosive components of wear.

Although we presented a detailed description of wear mechanisms regarding different counterbodies, this study was limited to not providing the synergism parcel between wear and corrosion, which will be a topic to be explored in a further investigation.

Author Contributions YIO, BCESK and VTM: experimental tests, prepared figures, GP: wrote the main manuscript text, conceptualization, XL and HSD: samples preparation and processing. All authors reviewed the manuscript.

Data Availability Data sets generated during the current study are available at http://repositorio.utfpr.edu.br/jspui/handle/1/4321.

Declarations

Conflict of Interest The authors have no competing interests to declare that are relevant to the content of this article.

References

1. Lu, X., Ma, Y., Wang, D.: On the hydrogen embrittlement behavior of nickel-based alloys: alloys 718 and 725. Mater. Sci. Eng. A **792**, 139785 (2020)

2. Houghton, A., Lewis, R., Olofsson, U., Sundh, J.: Characterising and reducing seizure wear of inconel and incoloy superalloys in a sliding contact. Wear **271**(9–10), 1671–1680 (2011)

3. Zhang, H., Qin, H., Ren, Z., Zhao, J., Hou, X., Doll, G.L., Ye, C.: Low-temperature nitriding of nanocrystalline Inconel 718 alloy. Surf. Coat. Technol. **330**, 10–16 (2017)

4. Xue, L., Wang, J., Li, L., Chen, G., Sun, L., Yu, S.: Enhancement of wear and erosion-corrosion resistance of Inconel 718 alloy by liquid nitriding. Mater. Res. Express. **7**(9), 096510 (2020)

5. Kovací, H., Ghahramanzadeh, A.S.L., Albayrak, Ç., Alsaran, A., Çelik, A.: Effect of plasma nitriding parameters on the wear resistance of alloy Inconel 718. Met. Sci. Heat. Treat. **58**(7), 470–474 (2016)

6. Maniee, A., Mahboubi, F., Soleimani, R.: Improved hardness, wear and corrosion resistance of inconel 718 treated by hot wall plasma nitriding. Metals Mater. Int. **26**, 1664–1670 (2019)

7. Mondragón-Rodríguez, G.C., Torres-Padilla, N., Camacho, N., Espinosa-Arbeláez, D.G., de León-Nope, G.V., González-Carmona, J.M., Alvarado-Orozco, J.M.: Surface modification and tribological behavior of plasma nitrided Inconel 718 manufactured via direct melting laser sintering method. Surf. Coat. Technol. **387**, 125526 (2020)

8. Singh, V., Meletis, E.I.: Synthesis, characterization and properties of intensified plasma-assisted nitrided superalloy Inconel 718. Surf. Coat. Technol. **201**(3–4), 1093–1101 (2006)

9. De Bartolomeis, A., Newman, S.T., Jawahir, I.S., Biermann, D., Shokrani, A.: Future research directions in the machining of Inconel 718. J. Mater. Proc. Technol. **297**, 117260 (2021)

10. Stachowiak, A., Wieczorek, D., Gruber, K., Bartkowski, D., Bartkowska, A., Ulbrich, D.: Comparison of tribocorrosion resistance of Inconel® 718 alloy manufactured by conventional method and laser powder bed fusion method. Tribol. Int. **182**, 108368 (2023)

11. Zhang, B., Xiu, M., Tan, Y.T., Wei, J., Wang, P.: Pitting corrosion of SLM Inconel 718 sample under surface and heat treatments. Appl. Surf. Sci. **490**, 556–567 (2019)

12. Nunez, Y., Mafra, M., Morales, R.E., Borges, P.C., Pintaude, G.: The effect of plasma nitriding on the synergism between wear and corrosion of SAF 2205 duplex stainless steel. Ind. Lub. Tribol. **72**(9), 1117–1122 (2020)

13. Nuñez de la Rosa, Y., Palma Calabokis, O., Ballesteros-Ballesteros, V., Tafur, C.L., Borges, P.C.: Assessment of the pitting, crevice corrosion, and mechanical properties of low-temperature plasma-nitrided inconel alloy 718. Metals **13**(7), 1172 (2023)

14. Sharma, S.K., Manoj Kumar, B.V., Kim, Y.W.: Tribology of WC reinforced SiC ceramics: influence of counterbody. Friction **7**(2), 129–142 (2019)

15. Anand Kumar, S., Sundar, R., Ganesh Sundara Raman, S., Gnanamoorthy, R., Kaul, R., Ranganathan, K., Bindra, K.S.: Effects of laser peening on fretting wear behavior of alloy 718 fretted against two different counterbody materials. Proc. Inst. Mech. Eng. Part J J. Eng. Tribol. **231**(10), 1276–1288 (2017)

16. Jing, Y., Jun, W., Tan, G., Ji, X., Hongyuan, F.: Phase transformations during low temperature nitrided Inconel 718 superalloy. ISIJ Int. **56**(6), 1076–1082 (2016)

17. Kurelo, B.C.S., de Souza, G.B., Serbena, F.C., Lepienski, C.M., Borges, P.C.: Mechanical properties and corrosion resistance of αN-rich layers produced by PIII on a super ferritic stainless steel. Surf. Coat. Technol. **403**, 126388 (2020)

18. Souza, G.B.D., Foerster, C.E., Silva, S.L.R.D., Lepienski, C.M.: Nanomechanical properties of rough surfaces. Mater. Res. **9**, 159–163 (2006)

19. Wollmann, D., Pintaude, G.: Tribological performance of high-strength cast iron in lubricated contact containing carbon black. Wear **476**, 203743 (2021)

20. US-ASTM. ASTM G59-97-2009 Standard Test Method for Conducting Potentiodynamic Polarization Resistance Measurements. ASTM 2009

21. Stinville, J.C., Templier, C., Villechaise, P., Pichon, L.: Swelling of 316L austenitic stainless steel induced by plasma nitriding. J. Mater. Sci. **46**(16), 5503–5511 (2011)

22. Chollet, S., Pichon, L., Cormier, J., Dubois, J.B., Villechaise, P., Drouet, M., Templier, C.: Plasma assisted nitriding of Ni-based superalloys with various microstructures. Surf. Coat. Technol. **235**, 318–325 (2013)

23. Pintaude, G.: Introduction of the ratio of the hardness to the reduced elastic modulus for abrasion. In: Gegner, J. (ed.) Tribology—fundamentals and advancements, pp. 217–230. IntechOpen, London (2013)

24. Fillot, N., Iordanoff, I., Berthier, Y.: Wear modeling and the third body concept. Wear **262**(7–8), 949–957 (2007)

25. Writzl, V., Rovani, A.C., Pintaude, G., Lima, M.S.F., Guesser, W.L., Borges, P.C.: Scratch resistances of compacted graphite iron with plasma nitriding, laser hardening, and duplex surface treatments. Tribol. Int. **143**, 106081 (2020)

26. Ghaednia, H., Pope, S.A., Jackson, R.L., Marghitu, D.B.: A comprehensive study of the elasto-plastic contact of a sphere and a flat. Tribol. Int. **93**, 78–90 (2016)

27. Basu, A., Majumdar, J.D., Alphonsa, J., Mukherjee, S., Manna, I.: Corrosion resistance improvement of high carbon low alloy steel by plasma nitriding. Mater. Lett. **62**(17–18), 3117–3120 (2008)

28. Chicot, D., Mendoza, J., Zaoui, A., Louis, G., Lepingle, V., Roudet, F., Lesage, J.: Mechanical properties of magnetite (Fe3O4), hematite (α-Fe2O3) and goethite (α-FeO·OH) by instrumented indentation and molecular dynamics analysis. Mater. Chem. Phys. **129**(3), 862–870 (2011)

29. Pintaude, G., Tanaka, D.K., Sinatora, A.: The effects of abrasive particle size on the sliding friction coefficient of steel using a spiral pin-on-disk apparatus. Wear **255**(1–6), 55–59 (2003)

30. Papageorgiou, N., Von Bonin, A., Espallargas, N.: Tribocorrosion mechanisms of NiCrMo-625 alloy: an electrochemical modeling approach. Tribol. Int. **73**, 177–186 (2014)

31. Espallargas, N., Mischler, S.: Dry wear and tribocorrosion mechanisms of pulsed plasma nitrided Ni–Cr alloy. Wear **270**(7–8), 464–471 (2011)

32. Varela, L.B., Ordoñez, M.F., Pinedo, C.E., Tschiptschin, A.P.: Micro-abrasive wear study of a low-temperature plasma nitrided Inconel 625 superalloy. Tribol. Mater. Surf. Interfaces **16**(2), 119–129 (2022)

33. Jun, C., Qing, Z., Jianzhang, W., Fengyuan, Y.: Electrochemical effects on the corrosion-wear behaviors of NiCrMo-625 alloy in artificial seawater solution. Tribol. Trans. **59**(2), 292–299 (2016)

34. López-Ortega, A., Arana, J.L., Bayón, R.: On the comparison of the tribocorrosion behavior of passive and non-passivating materials and assessment of the influence of agitation. Wear **456**, 203388 (2020)

35. Kasturibai, S., Kalaignan, G.P.: Pulse electrodeposition and corrosion properties of Ni–Si3N4 nanocomposite coatings. Bull. Mater. Sci. **37**(3), 721–728 (2014)

36. Woodward, R.G., Toumpis, A., Galloway, A., Sillars, F., Marrocco, T., Olasolo, M., Wallace, A.: The influence of load on dry and tribocorrosive sliding of AISI 4330 and 15–5PH against cast iron. Tribol. Trans. **64**(5), 956–967 (2021)